Supplementary Information (SI)

Data-driven synthesis of electron-rich metal-organic frameworks for enhanced U(VI) removal

Chongxiong Duan[a], Kai Zheng[a], Yu Liang[a], Yu Wang[a], Manqi Liu[a], Baiming Liang[a], Zemei Tan[a], Xuquan, Liu[a], Jinpeng Zhang[a], Chen Liu[b], Hongxia Xi[d], Pengfei Yang*[b], Xuejiao Sun*[c]

[a] School of Materials and Energy, Foshan University, Foshan 528231, P.R. China,

[b] School of Chemistry and Chemical Engineering, University of South China, Hengyang 421001, China,

[c] School of Chemical Engineering and Technology, Guangdong Industry Polytechnic, Guangzhou 510330, China,

[d] School of Chemistry and Chemical Engineering, South China University of Technology, Guangzhou 510640, China.

Experimental

Chemicals and reagents

All reagents were of analytical grade and obtained from commercial suppliers without further purification. Anhydrous ethanol (CH_3CH_2OH), zirconium tetrachloride ($ZrCl_4$), terephthalic acid (H_2BDC), N,N-dimethylformamide (DMF), 2-aminobenzene-1,4-dicarboxylic acid (BDC-NH2), ethylenediamine (ED), diethylenetriamine (DETA), acetic acid (HAc), and anhydrous toluene (PhMe) were purchased from Sinopharm chemical reagent Co., Ltd. (China). Arsenazo III of chemical purity has been derived from Guangzhou Jiangshun chemical technology Co., Ltd. (China). Hexahydrated uranium nitrate ($UO_2(NO_3)_2 \cdot 6H_2O$) was purchased from Xi 'an Dingtian chemical Co., Ltd. (China).

Characterization

The analysis of morphology was performed utilizing a scanning electron microscope (SEM, ZEISS Sigma300, Gemini) along with a transmission electron microscope (TEM, JEM-2100F). In addition, element distribution map (Mapping) was tested by SEM. X-ray diffraction (XRD) pattern of sample was recorded in continuous scanning mode on a diffractometer system (Rigaku SmartLab SE). The diffraction patterns were recorded within a scanning range of 5-90° using CuKα radiation. The samples underwent thermogravimetric analysis (TGA) on a TG analyzer (RIGAKU, TG-DTA8122, Thermo plus EVO2), being heated from 303 K to 1073 K in a N_2 atmosphere at a rate of 20 K min^{-1}. FTIR spectra were recorded with an FTIR spectrometer (Bruker ALPHA) at a resolution of 4 cm^{-1} and the attenuated total reflection (ATR) method was adopted. N_2 adsorption-desorption isotherm experiment of samples was performed on an ASAP 2460 (Micromeritics, USA) at 77 K. The calculation of the specific surface area was performed using Brunauer-Emmett-Teller (BET) method, and the distribution of pore sizes was assessed through the application of the nonlocal density functional theory (NL-DFT) approach. X-ray photoelectron spectroscopy (XPS, Thermo ESCALAB250 XI) was carried out to investigate surface chemical states. The concentration of U(VI) in solution was quantitatively determined using UV-visible spectroscopy with a T6 Xinrui spectrophotometer.

U(VI) adsorption experiments

To investigate the uranium adsorption performance of UiO-66 series materials, the following experiments were designed and conducted: the effects of pH value of the uranium solution, contact time, different initial concentrations of the uranium solution, and cyclic experiments under optimal adsorption conditions.

Prior to the experiments, a standard uranium solution ($UO_2(NO_3)_2 \cdot 6H_2O$) with a concentration of 1 g L^{-1} was prepared and subsequently diluted to specified concentrations (10-110 mg L^{-1}) using deionized water. The pH of the uranium solutions was adjusted to a range of 4-10 using 0.1 mol L^{-1} HCl and 0.1 mol L^{-1} NaOH solutions, respectively.

At 308 K, an adsorbent with a concentration of 80 mg L^{-1} was ultrasonically dispersed in 25 mL of uranium solution at a specific concentration, and the pH was adjusted accordingly. The resulting mixture was then transferred to a 50 mL conical flask and placed in a thermostatic shaker for continuous oscillation. After the oscillation was completed, the mixture was filtered through a membrane with a pore size of 0.22 μm.

Subsequently, the remaining uranium concentration in the solution was determined using UV-vis absorption spectroscopy, based on the characteristic absorption peak generated when the arsenazo III color reagent forms a complex with uranyl ions at a wavelength of 652 nm. The adsorption capacity of the adsorbent for uranium was calculated using Equation (1)[1]:

$$Q_e = \frac{(C_0 - C_t)V}{m} \quad (1)$$

Where Q_e (mg g^{-1}) is the equilibrium adsorption capacity of uranium, C_0 (mg L^{-1}) is the initial concentration of uranium, and C_t (mg L^{-1}) is the concentration of uranium at time *t*.

Adsorption kinetics and isotherms models

The linear shapes of pseudo-first-order, pseudo-second-order and M-W kinetic models were expressed as Equation (2), Equation (3) and Equation (4)[2]:

$$ln(Q_e - Q_t) = lnQ_e - k_1 t \quad (2)$$

$$\frac{t}{Q_t} = \frac{1}{Q^2{}_e k_2} + \frac{t}{Q_e} \quad (3)$$

$$Q_e = k_3\sqrt{t} + C \quad (4)$$

Where Q_t (mg g^{-1}) and Q_e (mg g^{-1}) are the adsorption capacity at time *t* (min) and the equilibrium adsorption capacity of uranium, respectively. k_1 (min^{-1}) represents the equilibrium rate constant of the pseudo first-order sorption. k_2 (g mg^{-1} min^{-1}) represents the equilibrium rate constant of the pseudo-second-order sorption. k_3 is the rate constant of intraparticle diffusion, and C is the rate constants of the Intra-particle diffusion model.

The fitting equations of the Langmuir model, Freundlich and Temkin model were shown in Equation (5), Equation (6) and Equation (7), respectively[3, 4]:

$$\frac{C_e}{q_e} = \frac{C_e}{Q_{max}} + \frac{1}{Q_{max}K_L} \quad (5)$$

$$lnq_e = lnK_F + \frac{1}{n}lnC_e \quad (6)$$

$$q_e = \frac{RT}{b_T}lnA_T + (\frac{RT}{b_T})lnC_e \quad (7)$$

Where C_e (mg L^{-1}) and q_e (mg g^{-1}) are the equilibrium concentration of uranium and the equilibrium adsorption capacity of uranium, respectively. Q_{max} (mg g^{-1}) is the theoretical maximum adsorption capacity of uranium adsorbed per unit mass of samples. k_L (L mg^{-1}) is the constant related to the Langmuir adsorption, and k_F is the constant related to the Freundlich adsorption. $\frac{1}{n}$ is an empirical parameter corresponding to surface heterogeneity or adsorption intensity. R is the gas constant (8.314 J mol^{-1} K^{-1}), b_T (J mol^{-1}) is the Temkin isotherm constant, which is related to the adsorption heat and reflects the variation of adsorption heat with coverage. A_T

is a constant related to the binding ability between the adsorbent and the adsorbate, and is usually associated with the number of active sites on the adsorbent.

Theoretical calculations

In this study, CoRE MOF24 database was selected for research purposes. Initially, the CIF files of MOFs within this database were converted into SMILES format using the Open Babel software to achieve standardized molecular structure representation. Subsequently, within the Anaconda environment, the RDKit toolkit was employed to generate MACCS molecular fingerprints, which are 166-bit binary-encoded descriptors of molecular substructural features. In accordance with our research requirements, we specifically targeted and selected MACCS fingerprint bits associated with electron-rich groups. These electron-rich groups encompass heteroatoms with lone pairs of electrons, conjugated π-systems, and electron-donating groups, among others. The selected MACCS fingerprint bits include MACCS_13, 15, 23, 24, 25, 36, 37, 40, 55, 57, 58, 60, 63, 71, 88, 94, 102, 109, 110, 121, 123, 137, 139, 151, 154, and 157. Finally, we tallied the number of MOFs corresponding to each of these selected fingerprint bits. This quantitative data will serve as a foundational support for subsequent investigations into the correlations between electron-rich groups and the properties of MOFs.

Quantum chemical calculations were conducted using the DFT method implemented in the Gaussian 16 (A.03) program. Geometric optimization and frequency analysis were carried out with the PBE0-D3BJ hybrid exchange-correlation functional, applying the SDD basis set for uranium and the def2-SVP basis set for light elements such as C, H, O, and N. All optimized structures were confirmed to exhibit no imaginary frequencies. The adsorption energies of UO_2^{2+} with UiO-66 series materials were computed as following[5]:

$$E_{ads} = E_{total} - E_{substrate} - E_{UO_2^{2+}} \quad (8)$$

Where E_{ads} is the adsorption energy, E_{total} is the energy of the adsorbent-adsorbate system after adsorption, $E_{substrate}$ is the energy of the pristine substrate, and $E_{UO_2^{2+}}$ corresponds to the energy of the uranyl ion.

In addition, to reduce computational cost while maintaining chemical relevance, all DFT calculations were performed using ligand-fragment models rather than full Zr_6-oxo cluster or periodic UiO-66 structures. Such fragment models have been widely used for evaluating local electronic properties and functional-group effects[6, 7]. Nevertheless, they cannot fully reproduce the steric environment, pore confinement, or long-range electrostatic field of the metal cluster nodes[8]. As a result, the reported adsorption energies should be interpreted as qualitative trends. The consistency between the theoretical trends and experimental adsorption capacities supports the validity of this simplified modeling strategy[9, 10].

Figures

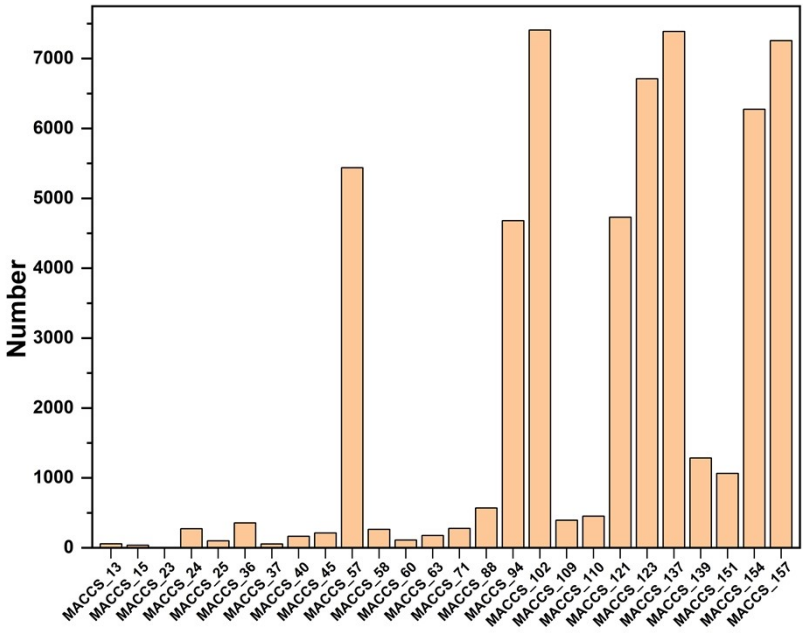

Fig. S1 Distribution of the number of MOFs with electron-rich groups in the Core MOF24 database.

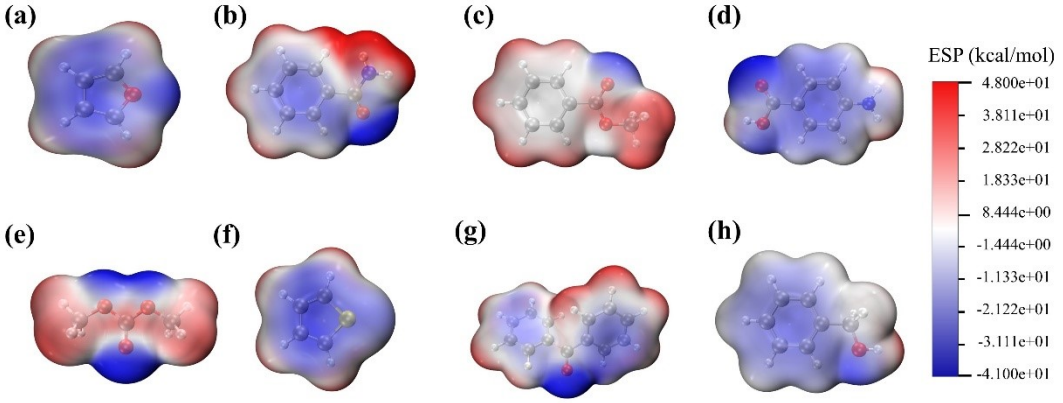

Fig. S2 Representative ESP maps of eight ligands selected from different electron-rich categories, used for the systematic comparison to identify the optimal functionalization strategy. ESP maps of (a) furan, (b) benzamide, (c) benzoate ester, (d) p-aminobenzoic acid, (e) dimethyl carbonate, (f) thiophene, (g) benzophenone, and (h) benzyl alcohol.

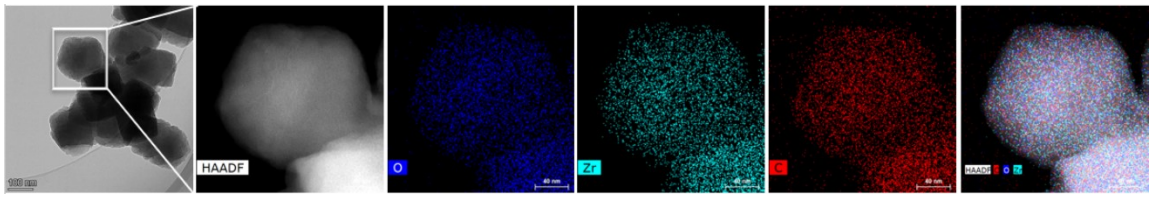

Fig. S3 The TEM and Mapping images of C-UiO-66: O, Zr, and C elemental.

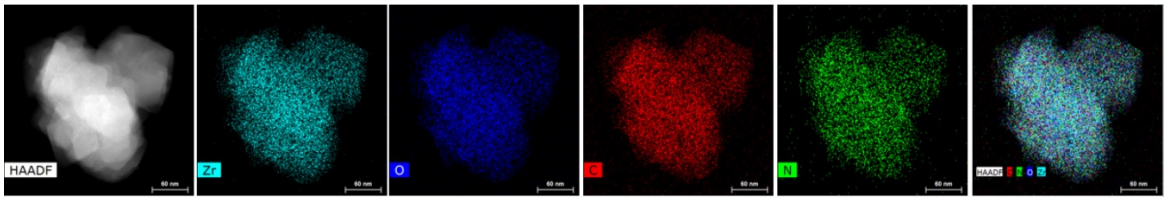

Fig. S4 The TEM and Mapping images of NH_2-UiO-66: Zr, O, C, and N elemental.

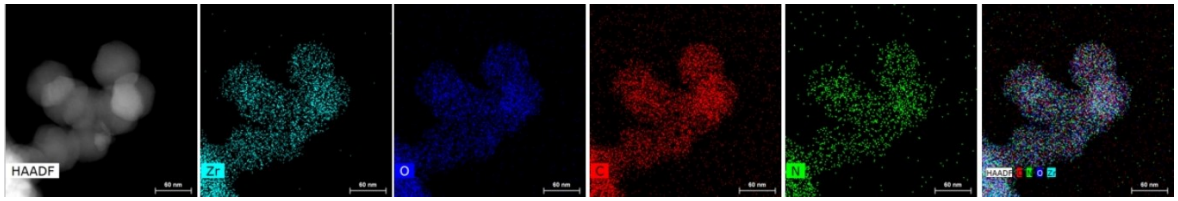

Fig. S5 The TEM and Mapping images of ED-UiO-66: Zr, O, C, and N elemental..

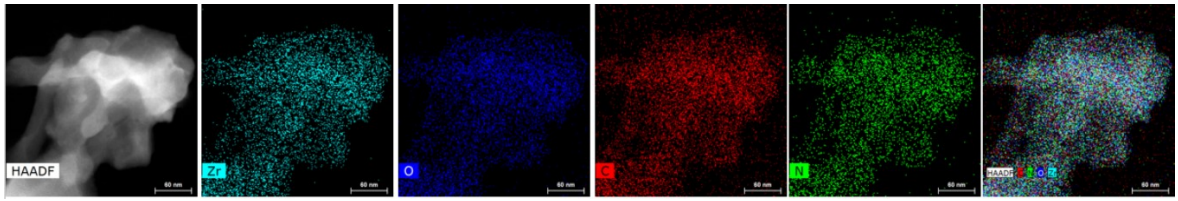

Fig. S6 The TEM and Mapping images of DETA-UiO-66: Zr, O, C, and N elemental..

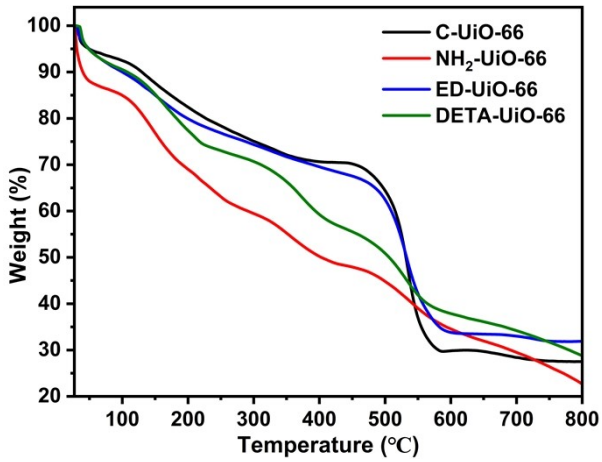

Fig. S7 The TGA curve of C-UiO-66, NH_2-UiO-66, ED-UiO-66 and DETA-UiO-66.

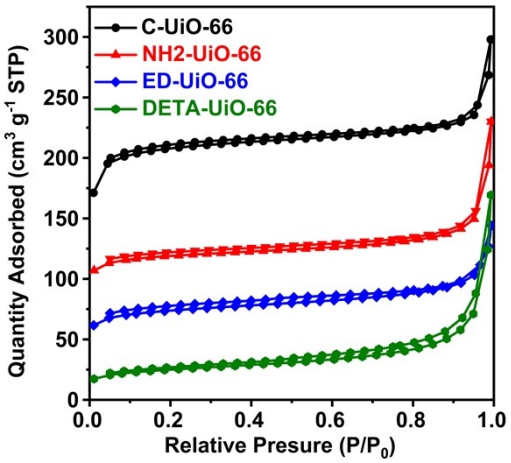

Fig. S8 N_2 adsorption-desorption isotherms of the as-synthesized UiO-66, NH_2-UiO-66, ED-UiO-66, and DETA-UiO-66.

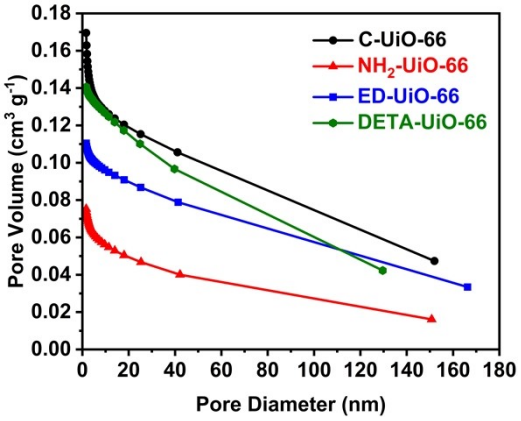

Fig. S9 The pore size distributions (PSD) of the as-synthesized UiO-66, NH_2-UiO-66, ED-UiO-66, and DETA-UiO-66.

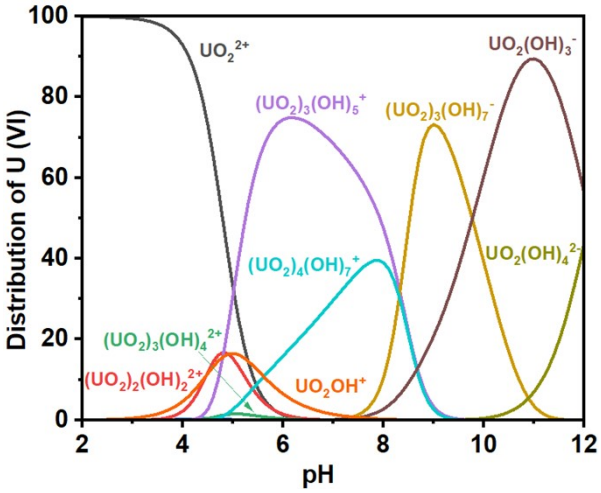

Fig. S10 The distribution of uranium species under different pH values (2-12).

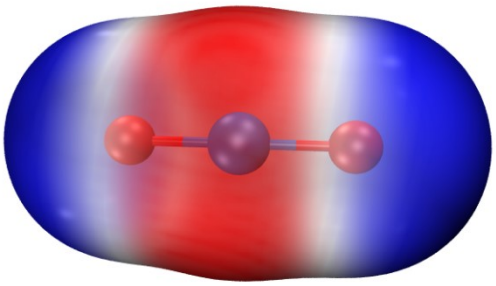

Fig. S11 The ESP maps of the UO_2^{2+}.

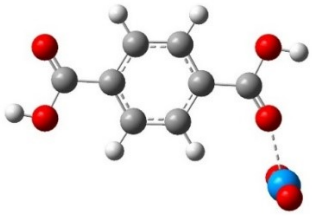

E_{ads}= -4.56 eV

Fig. S12 The optimal structure of the coordination complex between UO_2^{2+} and the ligands of C-UiO-66.

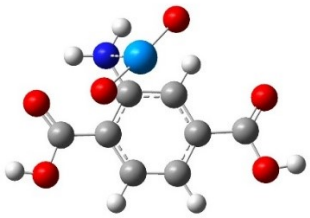

E_{ads}= -4.72 eV

Fig. S13 The optimal structure of the coordination complex between UO_2^{2+} and the ligands of NH_2-UiO-66.

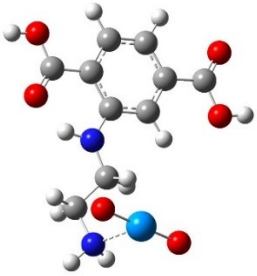

E_{ads}= -5.76 eV

Fig. S14 The optimal structure of the coordination complex between UO_2^{2+} and the ligands of ED-UiO-66.

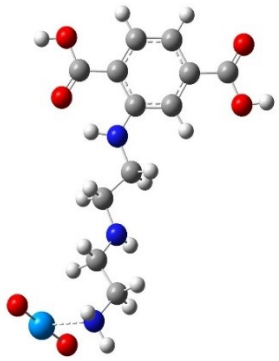

E_{ads}= -6.49 eV

Fig. S15 The optimal structure of the coordination complex between UO_2^{2+} and the ligands of DETA-UiO-66.

Tables

Molecular ACCess System (MACCS) fingerprints (166 kyes) were applied to describe the linker structures of MOFs[11].

Table S1 MACCS fingerprints and explanations[12].

No.	Explanation	No.	Explanation	No.	Explanation	No.	Explanation
1	ISOTOPE	43	QHAQH	85	CN(C)C	127	A$A!O > 1 (&...)
2	103 < ATOMIC NO. < 256	44	OTHER	86	CH2QCH2	128	ACH2AAACH2A
3	GROUP IVA,VA,VIA PERIODS 4-6 (Ge...)	45	C=CN	87	X!A$A	129	ACH2AACH2A
4	ACTINIDE	46	BR	88	S	130	QQ > 1 (&...)
5	GROUP IIIB,IVB (Sc...)	47	SAN	89	OAAAO	131	QH > 1
6	LANTHANIDE	48	OQ(O)O	90	QHAACH2A	132	OACH2A
7	GROUP VB,VIB,VIIB (V...)	49	CHARGE	91	QHAAACH2A	133	A$A!N
8	QAAA@1	50	C=C(C)C	92	OC(N)C	134	X (HALOGEN)
9	GROUP VIII (Fe...)	51	CSO	93	QCH3	135	Nnot%A%A
10	GROUP IIA (ALKALINE EARTH)	52	NN	94	QN	136	O=A > 1
11	4M RING	53	QHAAAQH	95	NAAO	137	HETEROCYCLE
12	GROUP IB,IIB (Cu...)	54	QHAAQH	96	5M RING	138	QCH2A > 1 (&...)
13	ON(C)C	55	OSO	97	NAAAO	139	OH
14	S-S	56	ON(O)C	98	QAAAAA@1	140	O > 3 (&...)
15	OC(O)O	57	O HETEROCYCLE	99	C=C	141	CH3 > 2 (&...)
16	QAA@1	58	QSQ	100	ACH2N	142	N > 1
17	CTC	59	Snot%A%A	101	8M RING	143	A$A!O
18	GROUP IIIA	60	S=O	102	QO	144	Anot%A%An

	(B...)						ot%A
19	7M RING	61	AS(A)A	103	CL	145	6M RING > 1
20	SI	62	A$A!A$A	104	QHACH2A	146	O > 2
21	C=C(Q)Q	63	N=O	105	A$A($A)$A	147	ACH2CH2A
22	3M RING	64	A$A!S	106	QA(Q)Q	148	AQ(A)A
23	NC(O)O	65	C%N	107	XA(A)A	149	CH3 > 1
24	N-O	66	CC(C)(C)A	108	CH3AAACH2A	150	A!A$A!A
25	NC(N)N	67	QS	109	ACH2O	151	NH
26	C$=C($A)$A	68	QHQH (&...)	110	NCO	152	OC(C)C
27	I	69	QQH	111	NACH2A	153	QCH2A
28	QCH2Q	70	QNQ	112	AA(A)(A)A	154	C=O
29	P	71	NO	113	Onot%A%A	155	A!CH2!A
30	CQ(C)(C)A	72	OAAO	114	CH3CH2A	156	NA(A)A
31	QX	73	S=A	115	CH3ACH2A	157	C-O
32	CSN	74	CH3ACH3	116	CH3AACH2A	158	C-N
33	NS	75	A!N$A	117	NAO	159	O > 1
34	CH2=A	76	C=C(A)A	118	ACH2CH2A > 1	160	CH3
35	GROUP IA (ALKALI METAL)	77	NAN	119	N=A	161	N
36	S HETEROCYCLE	78	C=N	120	HETEROCYCLIC ATOM > 1 (&...)	162	AROMATIC
37	NC(O)N	79	NAAN	121	N HETEROCYCLE	163	6M RING
38	NC(C)N	80	NAAAN	122	AN(A)A	164	O
39	OS(O)O	81	SA(A)A	123	OCO	165	RING
40	S-O	82	ACH2QH	124	QQ	166	FRAGMENTS
41	CTN	83	QAAAA@1	125	AROMATIC RING > 1		
42	F	84	NH2	126	A!O!A		

In MACCS keys, (1) atom symbols include: A (any valid periodic table element), Q (hetro atoms; any non-C or non-H atom), X (halogens), Z (other than H, C, N, O, Si, P, S, F, Cl, Br, I); (2) bond types include: - (single), = (double), T (triple), # (triple), ~ (single or double bond), % (aromatic bond), $ (ring), ! (chain or non-ring bond), @ (ring linkage and the number it specifies the atom position in the line).

Table S2 Surface area, pore volume and pore size of the C-UiO-66, NH_2- UiO-66, ED- UiO-66 and DETA-

UiO-66.

Sample	Surface area ($m^2 g^{-1}$)	Pore volume ($cm^3 g^{-1}$)	Pore size (nm)
C-UiO-66	818	0.675	2.0
NH_2-UiO-66	627	0.494	2.5
ED-UiO-66	336	0.382	2.0
DETA-UiO-66	205	0.299	5.0

Table S3 The Pseudo-second-order and Pseudo-first-order kinetics parameters onto C-UiO-66, NH_2-UiO-66, ED-UiO-66 and DETA-UiO-66.

Sample	Pseudo-first-order			Pseudo-second-order		
	k_1 (min)	Q_e (mg g^{-1})	R^2	k_2 (g mg^{-1} min^{-1})	Q_e (mg g^{-1})	R^2
C-UiO-66	0.0170±0.0021	431.81	0.917	0.00003±0.00014	284.90	0.956
NH_2-UiO-66	0.0198±0.0022	751.45	0.929	0.00003±0.00018	414.93	0.987
ED-UiO-66	0.0146±0.0023	402.90	0.864	0.00004±0.00023	512.82	0.994
DETA-UiO-66	0.0154±0.0021	315.06	0.896	0.00009±0.00049	520.83	0.999

Table S4 The Langmuir and Freundlich and Temkin isotherm parameters of C-UiO-66, NH_2-UiO-66, ED-UiO-66 and DETA-UiO-66.

Sample	T (K)	Langmuir isotherm			Freundlich isotherm			Temkin isotherm		
		Q_{max} (mg g^{-1})	K_L (L mg^{-1})	R^2	K (L g^{-1})	n	R^2	A_T	b_T(mol J^{-1})	R^2
C-UiO-66	308	213	0.75	0.999	124	6.4	0.505	995	125.5	0.629
NH_2-UiO-66	308	364	1.29	0.992	162	4.1	0.969	164	65.8	0.836
ED-UiO-66	308	481	1.63	0.989	283	6.7	0.873	1744	62.7	0.753
DETA-UiO-66	308	500	1.91	0.999	400	7.5	0.867	97086	71.0	0.856

Table S5 Adsorption capacity of various adsorbents for uranyl ion at 298 K.

Sample	Loading capacity ($mg \cdot g^{-1}$)	pH	Ref.
UIO-66-AO	227.8	5.0	[13]
P-UiO-66-AO	256.4	7	[14]
DUT-5-POR	263.4	6.0	[15]
HpZIF-8	297.7	4	[16]
DNPM	334.67	6	[17]
MIL-101(Cr)	350	4.5	[18]
ECUT-100	381	5.0	[19]
NiBDP-γ	430.8	5	[20]
SCU-19	557	3.0	[21]
USC-CP-1	562	5.5	[22]
C-UiO-66	212.8	7	This work
NH_2-UiO-66	347.1	7	This work
ED-UiO-66	462.5	7	This work
DETA-UiO-66	494.8	7	This work

References

1. T. Xiong, Q. Li, J. Liao, Y. Zhang and W. Zhu, *J. Hazard. Mater.*, 2022, **423**, 127184.
2. H. Li, J. Wang, J. Sun, P. Yang, S. Li, Z. Liu, C. Liu and C. Shen, *Chem. Eng. J.*, 2024, **497**, 154480.
3. P. Yang, Y. Xu, J. Tuo, A. Li, L. Liu and H. Shi, *R. Soc. Open Sci.*, 2019, **6**.
4. C. S. T. Araújo, I. L. S. Almeida, H. C. Rezende, S. M. L. O. Marcionilio, J. J. L. Léon and T. N. de Matos, *Microchem. J.*, 2018, **137**, 348-354.
5. K. Tuo, J. Li, Y. Li, C. Liang, C. Shao, W. Hou, C. Fan, Z. Li, S. Pu, Z. Chen and Y. Deng, *Small*, 2024, **21**.
6. Z. Wang, Z. Li, X.-G. Zhang, Q. Xia, H. Wang, C. Wang, Y. Wang, H. He, Y. Zhao and J. Wang, *ACS Appl. Mater. Interfaces*, 2021, **13**, 56025-56034.
7. J.-J. Cao, J.-L. Ge, Y. Gao and B.-K. Liao, *RSC Adv.*, 2025, **15**, 20570-20588.
8. S. O. Odoh, C. J. Cramer, D. G. Truhlar and L. Gagliardi, *Chem. Rev.*, 2015, **115**, 6051-6111.
9. J. L. Mancuso, A. M. Mroz, K. N. Le and C. H. Hendon, *Chem. Rev.*, 2020, **120**, 8641-8715.
10. P. Dobbelaere, S. Vandenhaute and V. Van Speybroeck, *Chem. Mater.*, 2025, **37**, 5696-5709.
11. J. L. Durant, B. A. Leland, D. R. Henry and J. G. Nourse, *J. Chem. Inf. Comput. Sci.*, 2002, **42**, 1273-1280.
12. Z. Zhang, A. S. Palakkal, X. Wu, J. Jiang and Z. Jiang, *Environ. Sci. Technol.*, 2025, **59**, 9123-9133.
13. J.-m. Liu, X.-h. Yin and T. Liu, *J. Taiwan Inst. Chem. Eng.*, 2019, **95**, 416-423.
14. L. Ma, C. Huang, Y. Yao, M. Fu, F. Han, Q. Li, M. Wu, H. Zhang, L. Xu and H. Ma, *Sep. Purif. Technol.*, 2023, **314**, 123526.
15. W. Wang, S. Ni, Y. Liu, Y. Zhao, Y. Meng and L. Yang, *Sep. Purif. Technol.*, 2024, **346**, 127409.
16. H. Zheng, X. Jiang, Y. Wang, G. Zhang, B. Zhang and Q. Zhang, *Colloid Surface A*, 2025, **716**, 136715.
17. J. Yu, J. Wang, H. Zhang, Q. Liu, J. Liu, J. Zhu, J. Yu and R. Chen, *Carbohyd. Polym.*, 2024, **323**, 121426.
18. F. Liu, S. Song, G. Cheng, W. Xiong, L. Shi and Y. Zhang, *Adsorpt. Sci. Technol.*, 2018, **36**, 1550-1567.
19. W. Zhang, A. Bu, Q. Ji, L. Min, S. Zhao, Y. Wang and J. Chen, *ACS Appl. Mater. Interfaces*, 2019, **11**, 33931-33940.
20. J. Li, N. Zhang, Q. Wang, B. Tian, Z. Li, J. Zhang, H. Xie, H. Gu and H. Zhao, *Chem. Eng. J.*, 2025, **515**, 163435.
21. M.-L. Feng, D. Sarma, X.-H. Qi, K.-Z. Du, X.-Y. Huang and M. G. Kanatzidis, *J. Am. Chem. Soc.*, 2016, **138**, 12578-12585.
22. X. F. Wang, Y. Chen, L. P. Song, Z. Fang, J. Zhang, F. Shi, Y. W. Lin, Y. Sun, Y. B. Zhang and J. Rocha, *Angew. Chem. Int. Ed. Engl.*, 2019, **58**, 18808-18812.